COMMUNICATIONS IN COMPUTATIONAL PHYSICS
Vol. **6**, No. 1, pp. 49-71

Commun. Comput. Phys.
July 2009

# Fast Numerical Simulation of Two-Phase Transport Model in the Cathode of a Polymer Electrolyte Fuel Cell

Pengtao Sun[1,*], Guangri Xue[2], Chaoyang Wang[3] and Jinchao Xu[2,4]

[1] *Department of Mathematical Sciences, University of Nevada, Las Vegas, 4505 Maryland Parkway, Las Vegas, NV 89154, USA.*
[2] *Department of Mathematics, The Pennsylvania State University, University Park, PA 16802, USA.*
[3] *Departments of Mechanical Engineering and Materials Science and Engineering, Electrochemical Engine Center (ECEC), The Pennsylvania State University, University Park, PA 16802, USA.*
[4] *Laboratory of Mathematics and Applied Mathematics, School of Mathematical Sciences, Peking University, Beijing 100871, China.*

Received 12 December 2007; Accepted (in revised version) 5 July 2008

Available online 13 November 2008

**Abstract.** In this paper, we apply streamline-diffusion and *Galerkin*-least-squares finite element methods for 2D steady-state two-phase model in the cathode of polymer electrolyte fuel cell (PEFC) that contains a gas channel and a gas diffusion layer (GDL). This two-phase PEFC model is typically modeled by a modified *Navier-Stokes* equation for the mass and momentum, with Darcy's drag as an additional source term in momentum for flows through GDL, and a discontinuous and degenerate convection-diffusion equation for water concentration. Based on the mixed finite element method for the modified *Navier-Stokes* equation and standard finite element method for water equation, we design streamline-diffusion and *Galerkin*-least-squares to overcome the dominant convection arising from the gas channel. Meanwhile, we employ *Kirchhoff* transformation to deal with the discontinuous and degenerate diffusivity in water concentration. Numerical experiments demonstrate that our finite element methods, together with these numerical techniques, are able to get accurate physical solutions with fast convergence.

**AMS subject classifications**: 65B99, 65K05, 65K10, 65N12, 65N22, 65N30, 65N55, 65Z05

**Key words**: Two-phase model, polymer electrolyte fuel cell, *Kirchhoff* transformation, convection dominated diffusion problem, streamline diffusion, *Galerkin*-least-squares.

*Corresponding author. *Email addresses:* pengtao.sun@unlv.edu (P. Sun), xue@math.psu.edu (G. Xue), cxw31@psu.edu (C. Wang), xu@math.psu.edu (J. Xu)

 ©2009 Global-Science Press

# 1 Introduction

Owing to their high energy efficiency, low pollution, and low noise, fuel cells are widely regarded as 21st century energy-conversion devices for mobile, stationary, and portable power. Through tremendous progress made in the past decade, currently available fuel cell materials appear to be adequate for near term markets with highest cost entry points. As a result, industries are currently placing their focus on fuel cell design and engineering for better performance, improved durability, cost reduction, and better cold-start characteristics. This new focus has led to an urgent need for identification, understanding, prediction, control, and optimization of various transport and electrochemical processes that occur on disparate length scales in fuel cells.

A fundamental fuel cell model consists of five principles of conservation [29]: mass, momentum, species, charge, and thermal energy. These transport equations are then coupled with electrochemical processes through source terms to describe reaction kinetics and electro-osmotic drag in the polymer electrolyte fuel cells (PEFC). Typically the fuel cell to be modeled is schematically shown in Fig. 1 and divided into seven subregions: the anode gas channel, anode gas diffusion layer (GDL), anode catalyst layer, ionomeric membrane, cathode catalyst layer, cathode gas diffusion layer (GDL), and cathode gas channel.

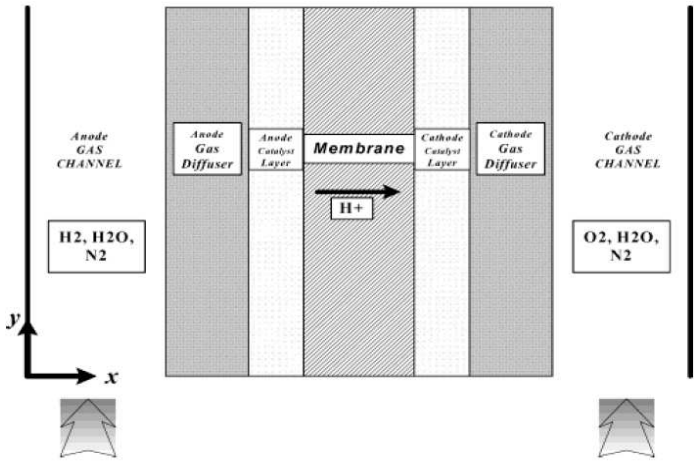


Figure 1: Schematic diagram of a polymer electrolyte fuel cell.

In this paper we specifically focus our interests on mass, momentum conservation and water concentration arising in gas channel and GDL of the cathode of PEFC. High-current-density operation of PEFCs, is prone to liquid water formation due to excessive water generation at the cathode, resulting in two-phase transport phenomena. The transport processes then become significantly more complicated due to the coupled flow of liquid water and gaseous reactants in porous media. Moreover, the ensuing two-phase transport of reactant and product species becomes a limiting mechanism for cell perfor-

mance, particularly at high current densities, i.e., greater than $1A/cm^2$. Therefore, a fundamental understanding of two-phase transport in porous gas diffusion layers of PEFCs is essential in order to improve cell performance.

Wang et al. [32] explored liquid water transport by capillary action, dynamic interaction between single- and two-phase zones via evaporation and condensation, and effects of the phase distribution on gas transport, and described a numerical study of gas-liquid, two-phase flow and transport in the air cathode of PEFC including hydrogen and direct methanol fuel cells. In their models, they employed a modified *Navier-Stokes* equation to describe the flow in gas channel and GDL simultaneously by adding a Darcy term in the source, so that gas channel is considered as completely permeable, while GDL is present as porous media. For water concentration equation, in order to present a unified model that encompasses both the single- and two-phase regimes, and ensures a smooth transition between the two, a discontinuous and degenerate function is introduced [32] as diffusivity of the transport equation in terms of water concentration. In gaseous water region, the water concentration is below a fixed value called saturated water concentration ($16mol/m^3$ at $80^\circ C$), coinciding with nonzero constant diffusivity. Once water concentration exceeds this fixed value, excess gaseous water is generated and condensed to liquid water. Correspondingly, the diffusivity suddenly jumps down to zero and then grows up into a smooth functional diffusivity with respect to liquid water concentration. Thus a degenerate and discontinuous diffusivity is induced. On the other hand, both momentum equation and concentration equation are all convection-dominated in gas channel due to the relative large velocity of gas flow.

To deeply investigate the numerical issue of two-phase PEFC models, without loss of generality, we adopt the models introduced by [32] and restrict it in two dimensional steady-state case. In this model the most difficult part is how to efficiently deal with the discontinuous and degenerate diffusivity arising in water concentration equation. Due to significant discontinuity, standard numerical discretization and linearization fail in obtaining stable convergent iteration for this nonlinear discontinuous and degenerate transport equation. The dominant convectional coefficient is another difficulty to get stable convergence for *Navier-Stokes* equation and convection-diffusion equation in gas channel.

Therefore, how to accurately and efficiently solve the modified *Navier-Stokes* equation and discontinuous and degenerate convection-diffusion problem with dominant convection terms are the fundamental numerical issues for two-phase transport model in the cathode of polymer electrolyte fuel cell, which is also the main goal of this paper.

The rest of this paper is organized as follows. First of all, the governing equations for two-phase steady-state transport problem in both gas channel and GDL are defined in Section 2. In Section 3, we introduce the method of *Kirchhoff* transformation [1, 2, 5, 7, 18, 33] and address how efficiently it deals with the discontinuous and degenerate diffusivity. The entire finite element discretizations is given in Section 4, where a type of mixed finite element method is employed to discretize momentum and continuity equations, and *Kirchhoff* transformation is adopted to solve the discontinuous and de-

generate water concentration equation. The dominant convection terms are dealt with by means of streamline-diffusion scheme [11, 12, 14, 17, 20] and *Galerkin*-least-squares scheme [8, 9, 25, 26]. Numerical simulations of several practical cases are illustrated in Section 5, indicating that our numerical schemes significantly improve the computational performance in efficiency as well as accuracy.

# 2 The 2D steady-state two-phase transport model in PEFC cathode

Based on [15], in this section we describe the governing equations for 2D steady-state two-phase transport problem in the cathode of PEFC, define the relevant physical parameters and coefficients, as well as their boundary conditions. All of the involved parameters refer to Table 1 in Section 2.2.

## 2.1 Governing equations

Specifically for 2D steady-state two-phase transport model in both gas channel and GDL, we introduce its governing equations in twofold fields: flow and species concentration.

**Flow equations.** For flow field with velocity $\vec{u}$ and pressure $P$ as unknowns, we have the following modified *Navier-Stokes* equations

$$\frac{1}{\varepsilon^2}\nabla\cdot(\rho\vec{u}\vec{u})=\nabla\cdot(\mu\nabla\vec{u})-\nabla P+S_u, \tag{2.1a}$$

$$\nabla\cdot(\rho\vec{u})=0, \tag{2.1b}$$

where $\varepsilon$ is porosity of air cathode, $\rho$ is density, $\mu$ is effective viscosity. We know (2.1b) is exact continuity equation, and (2.1a) represents a modified momentum equation, in which we indicate that the additional source term $S_u$ is named as Darcy's drag and defined as follows

$$S_u=-\frac{\mu}{K}\vec{u}, \tag{2.2}$$

where $K$ is a position-dependent "permeability" in porous cathode, defined as

$$K=\begin{cases} +\infty & \text{in gas channel,} \\ K_{\mathrm{GDL}}=10^{-12} & \text{in GDL.} \end{cases} \tag{2.3}$$

The definition of $K$ implies that gas channel is considered as completely permeable, while GDL is present as porous media with small permeability $K_{\mathrm{GDL}}$.

Darcy's drag $S_u$ is exactly developed from *Darcy*'s Law in porous GDL:

$$\vec{u}=-\frac{K_{\mathrm{GDL}}}{\mu}\nabla P.$$

When $K=\infty$ in gas channel, $S_u=0$ according to (2.2). Therefore (2.1a) reduces to classical momentum equation. On the other hand, notice that permeability $K_{\rm GDL}=10^{-12}$ and $\varepsilon=0.3$ in GDL, all the rest terms in (2.1a) in GDL become negligible after multiplying permeability $K$ on both sides, which induces (2.1a) to tend to be *Darcy*'s law along with a rescaled gradient pressure vector.

By virtue of this additional source term $S_u$, the momentum balance equation is modified to be valid in both GDL and gas channel, presenting the extended *Darcy*'s law for two-phase flow in porous GDL with small permeability, and exact *Navier-Stokes* equation in gas channel with unit porosity and infinite permeability. (2.1) is also known as *Darcy-Brinkman-Forchheimer* model [13], which is typically used to model the flow inside the porous domain. Finite difference method was first employed in [6] for such model involving the *Navier-Stokes* equations with an added Darcy term. Then a uniformly stable finite element method was developed in [34] with respect to the singularly perturbed coefficients for similar model.

The advantage of modified *Navier-Stokes* equation (2.1) is that, we simultaneously solve *Darcy-Navier-Stokes* flow in one single domain, instead of two-domain approach where *Beavers-Joseph-Saffman* interface condition [4, 10, 19] along the tangential direction of GDL/gas channel interface, continuity of mass flux and continuity of normal stress across GDL/gas channel interface must be employed. The equivalence between these two approaches is discussed in [21]. Obviously single domain approach is easier to implement, especially in the simulation of three dimensional complete fuel cell model, which will be investigated in separate paper [23].

**Species concentration equation.** Water management is one of the key issues in polymer electrolyte fuel cell. Due to the coexistence of single phase zone and two phase zone, water equation turns to be the most important and difficult species equation to deal with through the entire fuel cell. Therefore, for species concentration equations, in order to focus on water management topics, without loss of generality, we typically consider single component model by taking water as the only species in the simplified concentration equation.

Water concentration equations are spatially defined as follows with respect to water concentration $C$ [15]

$$\nabla\cdot(\gamma_c\vec{u}C)=\nabla\cdot(\Gamma(C)\nabla C), \quad \text{in GDL;} \tag{2.4a}$$

$$\nabla\cdot(\vec{u}C)=\nabla\cdot(D_g^{eff}\nabla C), \quad \text{in gas channel,} \tag{2.4b}$$

where $\gamma_c$ is the advection correction factor defined in Section 2.2, the diffusivity $\Gamma(C)$ in GDL is defined as

$$\Gamma(C)=\begin{cases}\Gamma_{capdiff}, & \text{if } C\geq C_{\rm sat};\\ D_g^{eff}, & \text{if } C<C_{\rm sat}.\end{cases} \tag{2.5}$$

Here $C_{\rm sat}$ is saturated water concentration. $D_g^{eff}=\varepsilon^{1.5}D_{gas}$ is the effective water vapor diffusivity, namely, the constant diffusivity in gaseous water region. $\Gamma_{capdiff}$ is capillary

diffusion coefficient, i.e. the functional diffusivity in liquid water region, defined as follows in terms of liquid saturation $s$:

$$\Gamma_{capdiff}=\left|\left(\frac{\mathrm{mf}_l}{M}-\frac{C_{\mathrm{sat}}}{\rho_g}\right)\left(\frac{M}{\rho_l-C_{\mathrm{sat}}M}\right)\frac{\lambda_l\lambda_g}{\nu}\sigma\cos\theta_c(\varepsilon K)^{1/2}\frac{dJ(s)}{ds}\right|, \tag{2.6}$$

here $s\in[0,1]$ denotes the liquid saturation throughout the paper. It is a basic variable in multiphase mixture ($M^2$) model [31, 32], and has coequality with water concentration as

$$C=\frac{\rho_l s}{M}+C_{\mathrm{sat}}(1-s),$$

hence

$$s=(C-C_{\mathrm{sat}})/(\frac{\rho_l}{M}-C_{\mathrm{sat}}).$$

$J(s)$ is the *Leverett* function, given by

$$J(s)=\begin{cases}1.417(1-s)-2.120(1-s)^2+1.263(1-s)^3, & \text{if } \theta_c<90^\circ;\\ 1.417s-2.120s^2+1.263s^3, & \text{if } \theta_c>90^\circ.\end{cases}$$

According to the definitions of physical parameters and coefficients in Section 2.2, we can easily calculate that $\Gamma_{capdiff}=0$ when $C=C_{\mathrm{sat}}$ or $s=0$. So $\Gamma_{capdiff}$, and further $\Gamma(C)$, is degenerate at $C_{\mathrm{sat}}$.

The behavior of diffusivity $\Gamma(C)$ can be better understood in Fig. 2, where $\Gamma(C)$ is clearly indicated as a discontinuous and degenerate function with respect to $C$. $C_{\mathrm{sat}}=16\ \mathrm{mol}/m^3$ is the typical point at which discontinuity and degeneracy occur for $\Gamma(C)$ at the same time.

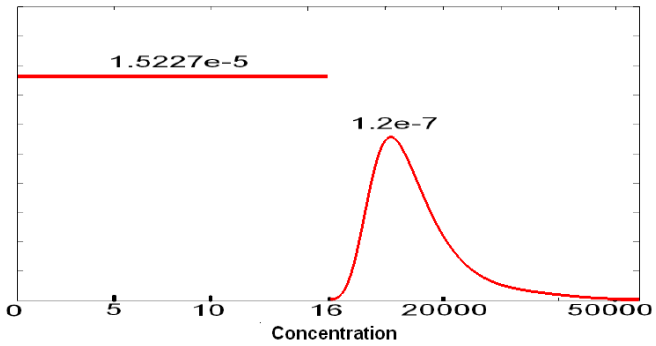


Figure 2: $\Gamma(C)$.

When the gas channel is dry, although there is huge jump in diffusivity $\Gamma(C)$ between the single- and two-phase regimes in GDL, $\Gamma(C)$ is still continuous across the GDL/gas channel interface due to the same constant diffusivity $D_g^{eff}$.

Governing equations (2.1) and (2.4), together with the definitions of physical coefficients and parameters in Section 2.2 and the boundary conditions in Section 2.3, constitute the 2D steady-state two-phase transport model in the cathode of polymer electrolyte fuel cell.

## 2.2 Coefficients and parameters

The physical coefficients and mixture variables arising in the governing equations (2.1), (2.4) and the definitions of their coefficients are specifically defined for single component two-phase transport PEFC model as follows:

- Density $\rho=\rho_l s+\rho_g(1-s)$,
- Relative mobilities $\lambda_l(s)=k_{rl}/\nu_l/(k_{rl}/\nu_l+k_{rl}/\nu_g)$ and $\lambda_g(s)=1-\lambda_l(s)$,
- Relative permeabilities $k_{rl}=s^3$ and $k_{rg}=(1-s)^3$,
- Kinematic viscosity $\nu=(k_{rl}/\nu_l+k_{rg}/\nu_g)^{-1}$,
- Effective viscosity $\mu=(\rho_l\cdot s+\rho_g\cdot(1-s)/(k_{rl}/\nu_l+k_{rg}/\nu_g)$,
- Advection correction factor $\gamma_c=(\rho(\lambda_l \mathrm{mf}_l+\lambda_g \mathrm{mf}_g))/(\rho_l \mathrm{mf}_l s+\rho_g \mathrm{mf}_g(1-s))$, where $\mathrm{mf}_l=1, \mathrm{mf}_g=C_{\mathrm{sat}}M/\rho_g$ are mass fractions of liquid water and gaseous water, respectively.

Advection correction factor $\gamma_c$ is a continuous function with respect to concentration. In gas channel we always assume water closes to be gaseous phase, i.e., $s=0$. Therefore, $\gamma_c$ is correspondingly reduced to be unity and the continuity of convectional coefficients of (2.4) are then preserved while crossing over the GDL/gas channel interface.

Other property parameters refer to Table 1.

Table 1: Property parameters.

| Parameter | Symbol | Value | Unit |
|---|---|---|---|
| Water vapor diffusivity | $D_{gas}$ | $2.6\times10^{-5}$ | $m^2/s$ |
| Water molecular weight | $M$ | 0.018 | $kg/mol$ |
| Vapor density | $\rho_g$ | 0.882 | $kg/m^3$ |
| Liquid water density | $\rho_l$ | 971.8 | $kg/m^3$ |
| Surface tension | $\sigma$ | 0.0625 | $kg/s^2$ |
| Contact angle between two phases | $\theta_c$ | $\frac{2}{3}\pi$ | |
| Porosity of GDL | $\varepsilon$ | 0.3 | |
| Kinematic liquid water viscosity | $\nu_l$ | $3.533\times10^{-7}$ | $m^2/s$ |
| Kinematic vapor viscosity | $\nu_g$ | $3.59\times10^{-5}$ | $m^2/s$ |
| Faraday constant | $F$ | 96487 | $A\cdot s/mol$ |
| Current density at the left end | $I_1$ | 20000 | $A/m^2$ |
| Current density at the right end | $I_2$ | 10000 | $A/m^2$ |

One advantage of multiphase mixture ($M^2$) model [30–32] is that we do not need to track phase interfaces between single- and two-phase regimes, it is automatically indicated by the solution, and therefore greatly simplifies numerical simulation of current two-phase transport problem. In fact, according to above definitions of coefficients, all

the governing equations (2.1), (2.4) identically reduce to their single-phase counterparts in the limits of the liquid saturation, $s$, equals to zero and unity, respectively.

## 2.3 Computational domain and boundary conditions

We specifically consider that governing equations (2.1) and (2.4) take place in the cathode of PEFC which consists of gas diffusion layer and opening gas channel, as schematically shown in Fig. 3. The horizontal $x$-axis represents the flow direction and the vertical $y$-axis points in the through-plane direction. The geometric sizes of this computational domain are marked in Fig. 3 as well, where the physical width of GDL and gas channel are $\delta_{\rm GDL}=3\times10^{-4}$ m, $\delta_{\rm CH}=10^{-3}$ m, respectively, in comparison with the length in flow direction $l_{\rm PEFC}=7\times10^{-2}$ m. The large aspect ratio of the channel length to width, which is up to about 1:100, exhibits a very micro-fabricated thin-film structure.

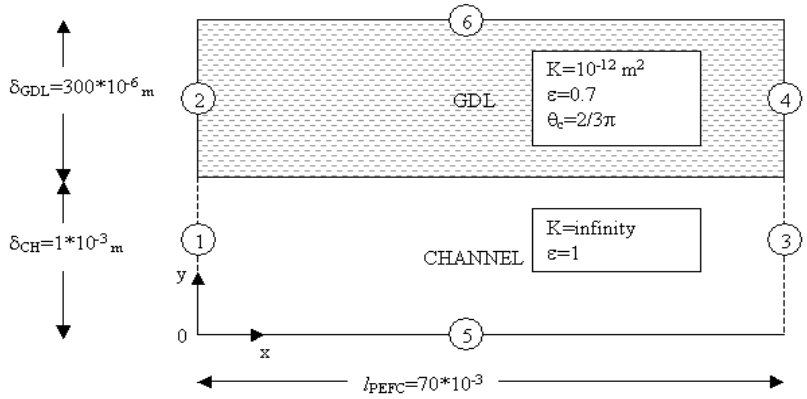


Figure 3: Domain.

At the inlet of the gas channel ($(\partial\Omega)_1$ in Fig. 3), constant flow rate and water concentration are specified. At the outlet ($(\partial\Omega)_3$ in Fig. 3), both velocity and concentration fields are assumed to be fully developed. Hence based on this computational domain, the boundary conditions are indicated as follows.

For flow field equation (2.1), the following boundary conditions hold with respect to velocity $\vec{u}$:

$$u_1=u_1|_{\rm inlet}(m/s), u_2=0 \quad \text{at inlet } (\partial\Omega)_1,$$

where $u_1|_{\rm inlet}$ are given in (4.8);

$$(P-\mu\nabla\vec{u})\cdot\vec{n}=0 \quad \text{at outlet } (\partial\Omega)_3;$$

$\vec{u}=0$ at the bottom wall $(\partial\Omega)_5$; $\vec{u}=0$ at side and top walls $(\partial\Omega)_2$,$(\partial\Omega)_4$ and $(\partial\Omega)_6$.

For water concentration (2.4), the following boundary conditions hold with respect to concentration $C$: at channel inlet $(\partial\Omega)_1$, $C=C_{\rm in}(mol/m^3)$; at the bottom and side walls

$(\partial\Omega)_2,(\partial\Omega)_3,(\partial\Omega)_4$ and channel outlet $(\partial\Omega)_5$, $\nabla C\cdot\vec{n}=0$; at the top wall $(\partial\Omega)_6$, the liquid water mass flux condition is given by:

$$\Gamma(C)\nabla C\cdot\vec{n}-\gamma_c\vec{u}C\cdot\vec{n}=\frac{I(x)}{2F}, \tag{2.7}$$

where the Dirichlet boundary condition at $(\partial\Omega)_1$ is usually set as $C_{\text{in}}<C_{\text{sat}}$ to indicate the input of gaseous component. At the membrane/cathode surface ($(\partial\Omega)_6$), the nonhomogeneous Neumann boundary condition is given to simulate oxygen reduction reaction occurring in catalyst layer and generating liquid water mass flux, which is demonstrated by *Faraday*'s law as shown in the right hand side of (2.7) [29], where $I(x)$ is the volumetric transfer current of the reaction (or transfer current density) defined by a linear function as follows

$$I(x)=\left(I_1-(I_1-I_2)\frac{x}{l_{\text{PEFC}}}\right)\left[\frac{A}{m^2}\right], \tag{2.8}$$

where $I_1$, $I_2$ are technically given in Table 1. (2.8) is the linear reduction of *Butler-Volmer* equation, indicates that the transfer current density linearly decreases from constant local current density $I_1$ at left end of membrane/cathode interface (top wall) to $I_2$ at right end. This is an approximation of transfer current density for our simplified single component two-phase PEFC model due to the absence of electric potentials.

## 3 *Kirchhoff* transformation

In this section, we start our numerical efforts with water concentration equation (2.4) first. Due to highly nonlinear discontinuous and degenerate diffusivity $\Gamma(C)$ defined in (2.5), it is hard to obtain convergent solution for the nonlinear iteration of (2.4) with standard finite element discretization. This nonconvergent phenomenon has been revealed by many numerical experiments with finite-volume based commercial flow solvers and our in-house code of standard finite element method [22], as shown in Fig. 4. Therefore, an efficient discretization scheme to deal with the nonlinear discontinuous and degenerate diffusivity $\Gamma(C)$ is the key to make the entire nonlinear iteration converge fast. To this end, by *Kirchhoff* transformation technique [1,2,5,7,18,33], we are able to reformulate (2.4) to a semilinear convection diffusion equation with simple *Laplacian* term as diffusion with respect to a new variable, where the nonlinearity, discontinuity and degeneracy arising in diffusivity $\Gamma(C)$ all disappear. Instead, we need to implicitly solve inverse *Kirchhoff* transformation in order to obtain the desired concentration.

First of all, based on diffusivity $\Gamma(C)$, we define a new variable $W$ in terms of *Kirchhoff* transformation

$$W(C)=\int_{C_{\text{min}}}^{C}\Gamma(\omega)d\omega. \tag{3.1}$$

Hence $W$ is a function of concentration $C\geq C_{\text{min}}$, where $C_{\text{min}}$ is the lower bound of concentration. Here we can take $C_{\text{min}}=C_{\text{in}}$, the entry concentration of gaseous water on the

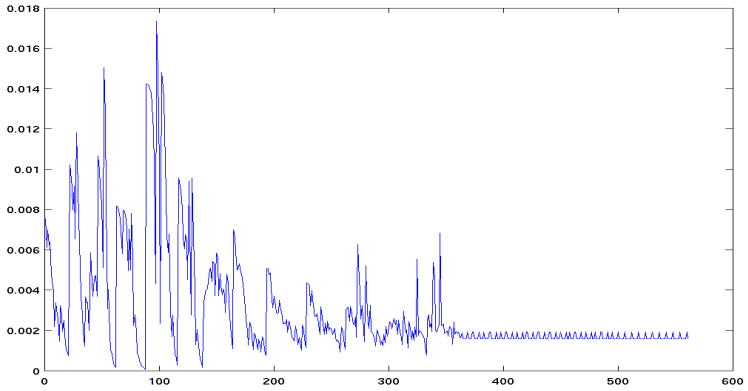


Figure 4: Convergence history with standard method for (2.4).

inlet. By minimum principle, $C_{\text{in}}$ is exactly the minimum concentration in the entire domain, if considering the positive water flux boundary condition on the top wall and zero source in (2.4), eventually positive total source for the entire domain.

On the contrary, it is impossible to find an explicit formula for inverse *Kirchhoff* transformation of (3.1) since concentration $C$ is a highly implicit function of $W$. A specific method needs to be found to compute $C$ from $W$.

In particular, for water concentration equation in gas channel (2.4b) with constant diffusivity $D_g^{eff}$, we still have the specific *Kirchhoff* transformation as follows

$$W=\int_{C_{\text{in}}}^{C} D_g^{eff}\,d\omega = D_g^{eff}(C-C_{\text{in}}), \tag{3.2}$$

where *Kirchhoff*'s variable $W$ is a linear function of $C$ in gas channel, or inversely,

$$C=(D_g^{eff})^{-1}W+C_{\text{in}}. \tag{3.3}$$

Thus the full *Kirchhoff* transformation for diffusivity $\Gamma(C)$ in water concentration equations (2.4) can be described as follows

$$W=\begin{cases} \int_{C_{\text{in}}}^{C}\Gamma(\omega)d\omega & \text{in GDL,} \\ D_g^{eff}(C-C_{\text{in}}) & \text{in Channel.} \end{cases} \tag{3.4}$$

Physically, we are looking at the dry channel case, i.e. the single-phase (gaseous water) region traverses GDL/gas channel interface and fills in the entire gas channel. Therefore $\Gamma(C)$ mathematically equals constant gas diffusivity $D_g^{eff}$ at the interface, which is consistent with the diffusivity in gas channel. Thus, the continuous solution $W$ is attained across the interface. By differentiating both sides of (3.1) with respect to spatial variables, we have the gradient of $W$: $\nabla W=\Gamma(C)\nabla C$.

By virtue of (3.4), and considering continuity equation (2.1b) in gas channel, we can reformulate (2.4) to an equivalent new water concentration equation with respect to $W$, along with new corresponding boundary conditions as follows

$$\Delta W = \nabla\cdot(\gamma_c\vec{u}C) \qquad \text{in GDL,} \tag{3.5a}$$

$$\Delta W = \nabla\cdot((D_g^{eff})^{-1}\vec{u}W) \qquad \text{in gas channel,} \tag{3.5b}$$

$$W = 0 \qquad \text{on } (\partial\Omega)_1, \tag{3.5c}$$

$$\frac{\partial W}{\partial n} - \gamma_c\vec{u}C\cdot\vec{n} = \frac{I}{2F} \qquad \text{on } (\partial\Omega)_6, \tag{3.5d}$$

$$\frac{\partial W}{\partial n} = 0 \qquad \text{elsewhere on } \partial\Omega. \tag{3.5e}$$

We observe that only one single *Laplacian* term is involved in the left hand side of (3.5a) and (3.5b), the original discontinuous and degenerate diffusivity $\Gamma(C)$ has been hidden inside the *Kirchhoff* transformation (3.1), which significantly reduces the difficulty of nonlinear iteration and makes fast convergence imaginable. Now the only nonlinearity stays in the right hand side of (3.5a), the convection term $\nabla\cdot(\gamma_c\vec{u}C(W))$, where $C$ is an implicit function of $W$ in terms of the inverse *Kirchhoff* transformation and the nonlinearity is introduced.

We notice that the convection term in GDL quite differs from that in gas channel. We reformulate them in different ways because of the significant distinction they bear on the convectional coefficients. On account of the linear inverse *Kirchhoff* transformation (3.3) in gas channel, we can directly get linear convectional coefficient for $W$ in (3.5b). But the inverse *Kirchhoff* transformation in GDL is implicitly given, no explicit formula to change variable $C$ to $W$ directly. On the other hand, it is hazardous if we insist on applying *Kirchhoff* transformation to $\nabla\cdot(\gamma_c\vec{u}C)$, a new convection term that explicitly depends on $W$ will be obtained as

$$\nabla\cdot(\gamma_c\vec{u}C) = \gamma_c\vec{u}\cdot\nabla C + \nabla\cdot(\gamma_c\vec{u})C = \gamma_c\vec{u}\cdot\frac{\nabla W}{\Gamma(C)} + \nabla\cdot(\gamma_c\vec{u})C(W).$$

As a result, a large or even infinite convection term $\nabla W/\Gamma(C)$ may be produced when $C$ is close to the degenerate point $C_{\text{sat}}$ and then $\Gamma(C)$ approaches zero. Therefore we must avoid applying *Kirchhoff* transformation to the convection term in (3.5a). Thanks to relatively very small *Darcy*'s velocity $\vec{u}$ in GDL in comparison with flow velocity in opening gas channel, this convection term is not dominant at all, accordingly we are able to keep its original form unchanged and move it to the right hand side as equivalent source term. This additional source term does not explicitly depend on $W$, which allow us to directly compute it by updating $C$ from the latest $W$ in terms of a doable inverse *Kirchhoff* transformation of (3.1).

Actually (3.5a) is only a semilinear equation because there is one single $C$ stays in the right hand side which depends on $W$ via the inverse *Kirchhoff* transformation, an implicit function. *Picard*'s method is sufficient to linearize it. In each iteration step, $C$ is updated

by the inverse *Kirchhoff* transformation from $W$. In contrast to (3.5a), (3.5b) is just a linear equation in gas channel, velocity $\vec{u}$ is remarkably large therein, which results in dominant convection term in (3.5b). So we cannot consider the preformation of convection term $\nabla\cdot((D_g^{eff})^{-1}\vec{u}W)$ as an additional source term. It has to be reformulated to current explicit convection form of $W$ via linear *Kirchhoff* transformation (3.3) and treated by certain upwind scheme in its discretization in order to stabilize the numerical solution.

In view of the weak nonlinearity in (3.5), we would be able to expect fast convergence of nonlinear iteration for $W$, and consequently for $C$, if an accurate and efficient method could carry the inverse *Kirchhoff* transformation of (3.1) into effect. It is nontrivial to compute this inverse *Kirchhoff* transformation directly [27,28]. One relatively simple approach is Look-Up Table (LUT) method, namely, search corresponding value of $C$ in a sorted relational data table between $W$ and $C$ at certain value of $W$ by one data search method, say, bisection. For more accurate and faster approach, see [24] where we present a type of *Newton*'s method to efficiently deal with the inverse *Kirchhoff* transformation.

# 4 Finite element approximations

In this section we design our finite element discretizations for *Navier-Stokes* equation (2.1) and the reformulated water concentration equation (3.5). Considering their various nonlinearities, we particularly employ *Newton*'s method to linearize the nonlinear convection term in (2.1) and *Picard*'s scheme to linearize the nonlinear source term in (3.5).

## 4.1 *Newton*'s linearization for *Navier-Stokes* equation (2.1)

Before *Newton*'s linearization, we rewrite (2.1) as following equivalent forms by applying continuity equation (2.1b) to the convection term in momentum equation (2.1a), and then splitting continuity equation to two parts in order to constitute a saddle point system:

$$\frac{\rho}{\varepsilon^2}\vec{u}\cdot\nabla\vec{u}=\nabla\cdot(\mu\nabla\vec{u})-\nabla P-\frac{\mu}{K}\vec{u}, \tag{4.1a}$$

$$\nabla\cdot\vec{u}=-\frac{\nabla\rho}{\rho}\cdot\vec{u}, \tag{4.1b}$$

*Newton*'s linearization for (4.1) follows thereafter. Provided $(\vec{u}^n,C^n)$ are given, we define $(\vec{u}^{n+1},P^{n+1})$ as the iterative solutions of the following *Newton*'s linearization scheme ($n=0,1,2,\cdots$):

$$\begin{aligned}&\frac{\rho^n}{\varepsilon^2}(\vec{u}^n\cdot\nabla\vec{u}^{n+1}+\nabla\vec{u}^n\cdot\vec{u}^{n+1})\\&\quad=\nabla\cdot(\mu^n\nabla\vec{u}^{n+1})-\nabla P^{n+1}-\frac{\mu^n}{K}\vec{u}^{n+1}+\frac{\rho^n}{\varepsilon^2}\vec{u}^n\cdot\nabla\vec{u}^n,\end{aligned} \tag{4.2a}$$

$$\nabla\cdot\vec{u}^{n+1}=-\frac{\nabla\rho^n}{\rho^n}\cdot\vec{u}^n. \tag{4.2b}$$

If the above scheme converges, then we can pass the limit $n\to\infty$ on both sides of (4.2). Since $\vec{u}^n\to\vec{u},\rho^n\to\rho,\mu^n\to\mu$, the limit of (4.2) is eventually equivalent to (4.1), the validity of linearization scheme (4.2) is confirmed.

### 4.2 *Picard*'s linearization for concentration equation (3.5)

Given $(\vec{u}^n,C^n)$, we define $(W^{n+1},C^{n+1})$ as the iterative solution of the following *Picard*'s linearization scheme ($n=0,1,2,\cdots$):

$$\begin{cases}\Delta W^{n+1}=\nabla\cdot(\gamma_c\vec{u}^nC^n) & \text{in GDL,}\\ \Delta W^{n+1}=\nabla\cdot((D_g^{eff})^{-1}\vec{u}^nW^{n+1}) & \text{in gas channel,}\end{cases}\tag{4.3}$$

together with the inverse *Kirchhoff* transformation, we obtain $C^{n+1}$ from $W^{n+1}$.

### 4.3 Weak forms

We define

$$\begin{aligned}&V:=\{\vec{v}=(v_1,v_2)^\top\in[H^1]^2\big|v_1|_{(\partial\Omega)_1}=u_1|_{\text{inlet}}\},\\&Q:=\{w\in H^1\big|w|_{(\partial\Omega)_1}=0\},\quad P:=L^2,\\&\widetilde{V}:=\{\vec{v}=(v_1,v_2)^\top\in[H^1]^2\big|v_1|_{(\partial\Omega)_1}=0\}.\end{aligned}$$

Then the mixed weak forms of (4.1) and (3.5) on the basis of linearizations (4.2) and (4.3) are presented as follows: for any $(\vec{v},q,w)\in\widetilde{V}\times P\times Q$, find $(\vec{u}^{n+1},P^{n+1},W^{n+1})\in V\times P\times Q$, such that

$$\begin{aligned}&(\mu^n\nabla\vec{u}^{n+1},\nabla\vec{v})+(\frac{\rho^n}{\varepsilon^2}\vec{u}^n\cdot\nabla\vec{u}^{n+1},\vec{v})+(\frac{\rho^n}{\varepsilon^2}\nabla\vec{u}^n\cdot\vec{u}^{n+1},\vec{v})\\&\quad-(P^{n+1},\nabla\cdot\vec{v}+(\frac{\mu^n}{K}\vec{u}^{n+1},\vec{v})=(\frac{\rho^n}{\varepsilon^2}\vec{u}^n\cdot\nabla\vec{u}^n,\vec{v}),&\text{(4.4a)}\\&-(\nabla\cdot\vec{u}^{n+1},q)=(\frac{\nabla\rho^n}{\rho^n}\cdot\vec{u}^n,q),&\text{(4.4b)}\\&(\nabla W^{n+1},\nabla w)=(\gamma_c\vec{u}^nC^n,\nabla w)+\int_{(\partial\Omega)_6}\frac{I(x)}{2F}wdx\quad\text{in GDL,}&\text{(4.4c)}\\&(\nabla W^{n+1},\nabla w)-((D_g^{eff})^{-1}\vec{u}^nW^{n+1},\nabla w)\\&\quad+\int_{(\partial\Omega)_3}(D_g^{eff})^{-1}\vec{u}^n\cdot\vec{n}W^{n+1}wdy=0\quad\text{in gas channel.}&\text{(4.4d)}\end{aligned}$$

### 4.4 Finite element discretization

In correspondence with mixed weak forms (4.4), we employ mixed finite element method to discretize *Navier-Stokes* equations (4.1), and apply standard finite element method to

reformulated water concentration equation (3.5) as well. Considering the convection term in (4.1a) and (3.5b) could be dominant due to the large velocity $\vec{u}$ in gas channel, therefore, in order to stabilize the numerical computation for nonlinear iteration (4.2) and (4.3), we need certain upwind scheme to overcome these possibly dominant convection terms.

Since finite-difference based upwind scheme cannot directly work for finite element discretization, as substitutes, streamline-diffusion scheme [11,12,14,17,20] and *Galerkin*-least-squares scheme [8,26] are appropriately chosen to deal with dominant convectional coefficients in the framework of finite element method. Typically, we apply *Galerkin*-least-squares scheme to (4.1a) and streamline-diffusion scheme to (3.5b), respectively, due to their own specific convective features. In our another paper [24], we will discuss a combined finite element-upwind finite volume method for this nonlinear convection-diffusion problem by employing a finite-volume based upwind scheme to specifically deal with dominant convection term only.

To discretize weak forms (4.4) via finite element method in the domain shown in Fig. 3, we firstly define the finite element space $S_h = V_h \times P_h \times Q_h \subset V \times P \times Q$ on certain uniform or quasi-uniform triangulation $\mathcal{T}_h$, where $V_h$ consists of piecewise quadratic polynomials, and $P_h$ and $Q_h$ consist of piecewise linear polynomials, $h$ represents the maximum mesh size. In $S_h$, subspace $V_h \times P_h$ is exactly the well known space of Taylor-Hood element, one type of stable mixed finite element specifically for saddle-point variational problem [3]. The purpose of such choice for finite element space $S_h$ is to approximate velocity with quadratic element ($P_2$), and pressure and concentration with linear element ($P_1$), simultaneously, on the theoretical basis of *Babuska-Brezzi-Ladyzhenskaya* condition (BBL) and its discrete form [16].

Based on weak forms (4.4), we define the following mixed finite element discretization, combining with *Galerkin*-least-squares and streamline-diffusion schemes together to deal with the dominant convection terms in momentum equation and concentration equation, respectively.

For any given $(\vec{v},q,w) \in S_h$, find $(\vec{u}_h^{n+1}, P_h^{n+1}, W_h^{n+1}) \in S_h$ $(n = 0,1,2,\cdots)$, such that

$$\begin{aligned}
&((\mu(C_h^n)\nabla\vec{u}_h^{n+1},\nabla\vec{v}) + (\frac{\rho(C_h^n)}{\varepsilon^2}\vec{u}_h^n\cdot\nabla\vec{u}_h^{n+1},\vec{v}) \\
&\quad + (\frac{\rho(C_h^n)}{\varepsilon^2}\nabla\vec{u}_h^n\cdot\vec{u}_h^{n+1},\vec{v}) - (P_h^{n+1},\nabla\cdot\vec{v}) + (\frac{\mu(C_h^n)}{K}\vec{u}_h^{n+1},\vec{v}) \\
&\quad + \delta_{gls}(h)\cdot\Big(\mathcal{L}(\vec{u}_h^{n+1},P_h^{n+1},W_h^{n+1}),\mathcal{L}(\vec{v},q,w)\Big) = (\frac{\rho(C_h^n)}{\varepsilon^2}\vec{u}_h^n\cdot\nabla\vec{u}_h^n,\vec{v}), \qquad (4.5a)\\
&-(\nabla\cdot\vec{u}_h^{n+1},q) = (\frac{\nabla\rho(C_h^n)}{\rho(C_h^n)}\cdot\vec{u}_h^n,q), \qquad (4.5b)\\
&(\nabla W_h^{n+1},\nabla w) = (\gamma_c\vec{u}_h^n C_h^n,\nabla w) + \int_{(\partial\Omega)_6}\frac{I(x)}{2F}w dx \quad \text{(GDL)}, \qquad (4.5c)
\end{aligned}$$

$$(\nabla W_h^{n+1},\nabla w)-((D_g^{eff})^{-1}\vec{u}_h^n W_h^{n+1},\nabla w)+\int_{(\partial\Omega)_3}(D_g^{eff})^{-1}\vec{u}_h^n\cdot\vec{n}W_h^{n+1}wdy$$
$$+\delta_{sld}(h)\left((D_g^{eff})^{-1}\vec{u}_h^n\cdot\nabla W_h^{n+1},(D_g^{eff})^{-1}\vec{u}_h^n\cdot\nabla w\right)$$
$$-\delta_{sld}(h)\left((D_g^{eff})^{-1}\frac{\nabla\rho(C_h^n)}{\rho(C_h^n)}\cdot\vec{u}_h^n W_h^{n+1},(D_g^{eff})^{-1}\vec{u}_h^n\cdot\nabla w\right)=0 \quad \text{(Gas channel)}, \tag{4.5d}$$

where the last term in the left hand side of (4.5a) is a stabilizing term, derived from *Galerkin*-least-squares scheme in terms of $\mathcal{L}$, which is the momentum operator of (4.1) and defined as

$$\mathcal{L}(\vec{u},P,W)=-\nabla\cdot(\mu(C(W))\nabla\vec{u})+\frac{\rho(C(W))}{\varepsilon^2}\vec{u}\cdot\nabla\vec{u}+\nabla P+\frac{\mu(C(W))}{K}\vec{u}.$$

This stabilizing term added is obtained by minimizing the sum of the squared residual of the momentum equation integrated over each element domain. It involves the momentum equation as a factor, therefore, despite this additional term, an exact solution is still admissible to the variational formulation given by (4.4).

Similarly, the streamline-diffusion scheme introduces the last term in the left hand side of (4.5d). Both of these two schemes aim at balancing the magnitudes between dominant convection term and insignificant diffusion term by working together with two important parameters $\delta_{gls}(h)$ and $\delta_{sld}(h)$. Although they present different forms, both of them intend to introduce artificial diffusivity (viscosity) into the discretization. To execute this mission, besides the additional discrete diffusive forms as shown above, parameters $\delta_{gls}(h)$ and $\delta_{sld}(h)$ play another important role here. Basically they hold

$$\delta_{gls}(h)=C_{gls}h,\quad \delta_{sld}(h)=C_{sld}h,$$

i.e., $\delta_{gls}(h)$ and $\delta_{sld}(h)$ are proportional to mesh size $h$, $C_{gls}$ and $C_{sld}$ are certain constant parameters. Therefore, when mesh size $h$ is sufficiently small, the additional diffusive terms introduced by *Galerkin*-least-squares and streamline-diffusion schemes eventually approximate to zero with the rate of convergence $\mathcal{O}(h)$. So numerical discretization (4.5) still approaches the original one when $h$ is small enough.

In practice, it is difficult to give a generic formula for $C_{gls}$ and $C_{sld}$ in nonlinear case [11, 12, 14, 17, 20]. They have to be chosen artificially in order to obtain the optimal stable solutions. Usually starting with small ones, we gradually increase the values of $C_{gls}$ and $C_{sld}$ and compute the corresponding finite element equations (4.5) until gained numerical solutions are not oscillating any more in convection-dominated opening gas channel.

We state the algorithm of implementing finite element discretizations (4.5) in Algorithm 4.1.

In Algorithm 4.1, we need to indicate the initial guesses $(\vec{u}_h^0,C_h^0)$. Although there is no certain way to define the initial guess, in practice, usually it can be simply given in terms of boundary conditions and physical phenomena. It is well known that the flow profile is parabolic once laminar flow is fully developed in long, straight channel, under steady

Algorithm 4.1:

For $n\geq 0$, given $\vec{u}_h^0, C_h^0$, the following procedures are successively executed:

1. Implicitly solve (4.5) for $(\vec{u}_h^{n+1}, P_h^{n+1}, W_h^{n+1})$ first.
2. Calculate $C_h^{n+1}$ with $W_h^{n+1}$ in terms of the inverse *Kirchhoff* transformation.
3. Determine if the following stopping criteria hold:

$$\frac{\|\vec{u}_h^{n+1}-\vec{u}_h^n\|_{L^2(\Omega)}+\|P_h^{n+1}-P_h^n\|_{L^2(\Omega)}+\|C_h^{n+1}-C_h^n\|_{L^2(\Omega)}}{\|\vec{u}_h^n\|_{L^2(\Omega)}+\|P_h^n\|_{L^2(\Omega)}+\|C_h^n\|_{L^2(\Omega)}}<\text{tolerance}, \tag{4.6}$$

which is the relative convergence error in successive two iteration steps. If yes, then numerical simulation is done. Otherwise, go back to the first step and continue.

flow conditions. Based on this fact, we are able to assign the initial data of velocity as follows

$$\begin{aligned}(u_h^0)_1&=\begin{cases} u_{\text{in}}\sin(y\pi/\delta_{\text{CH}}), & x=0,\ 0\leq y\leq\delta_{\text{CH}}\ (\text{inlet}),\\ 0, & \text{elsewhere},\end{cases}\\ (u_h^0)_2&=0,\quad C_h^0=C_{\text{in}},\end{aligned} \tag{4.7}$$

where $(u_h^0)_1$ is the $x$-component of $\vec{u}_h^0$. We use a sin function to approximate $(u_h^0)_1$ as a parabolic-like function at the inlet, an approximation of laminar flow in long, straight gas channel, whose the highest velocity $u_{\text{in}}$ (m/s) occurs at the center of inlet ($y=\delta_{\text{CH}}/2$) and quadratically decays to zero on the boundary wall. This initial guess is close to the real case of parabolic flow in relative long gas channel. It would be helpful to attain good convergence for nonlinear iteration accordingly. As a consequence, in the following numerical experiments, we assign the *Dirichlet* boundary condition of velocity at the inlet as follows

$$u_1|_{\text{inlet}}=u_{\text{in}}\sin(y\pi/\delta_{\text{CH}}),\quad 0\leq y\leq\delta_{\text{CH}}. \tag{4.8}$$

Considering *Kirchhoff* transformation (3.1) does not depend on the spatial domain but only concentration variable, we can directly generalize it to three dimensional case. Consequently numerical discretizations (4.5) are also able to be equivalently extended to three dimensional PEFC model without any difficulty.

In Section 5, a dry inlet will be chosen as a case of study therein because of recent interests in proton exchange membrane fuel cells (PEMFC) without external humidification and low-humidity, self-sustaining fuel cells for portable electronics. In addition, the dry inlet of the air cathode is of potential relevance to direct methanol fuel cell (DMFC). Thus the entire numerical methods studied in this section can be applied to this dry case immediately.

## 5 Numerical simulations

In practice, the magnitudes of imported velocity and concentration at the inlet of gas channel produce dramatic affection to velocity and water concentration field in both gas channel and GDL. Smaller concentration ($C_{\text{in}} < C_{\text{sat}}$) and bigger entry velocity ($u_{\text{in}} \geq 3m/s$), which imply dry air and fast vapor transport rate, may have greater possibility to keep gas channel dry than the other way round. On the other hand, higher transfer current density $I$ makes cathode reaction require more oxygen and generate more liquid water at membrane/cathode surface, which increases the amount of liquid water present in GDL and clearly forms the two-phase region. When accumulated liquid water in GDL drives the interface of single- and two-phase regions reaches over GDL/gas channel interface, wetted gas channel is produced accordingly.

In this section, we will illustrate these physical phenomena with the numerical methods mentioned in Section 4 by imposing various physical entry velocities at the inlet and transfer current densities $I$ at membrane/cathode surface $(\partial\Omega)_6$. Simultaneously the efficiency and accuracy of our presented numerical techniques are exhibited.

First of all, we define the triangulation $\mathcal{T}_h$ on the domain shown in Fig. 3 with 20 intervals for the length of fuel cell along $x$-direction, 30 and 25 intervals for the width of gas channel and GDL, respectively, along $y$-direction. So the number of total grids in $\mathcal{T}_h$ is $20\times(30+25)=1100$. The tolerance of our stopping criteria (4.6) for the nonlinear iteration is $10^{-10}$.

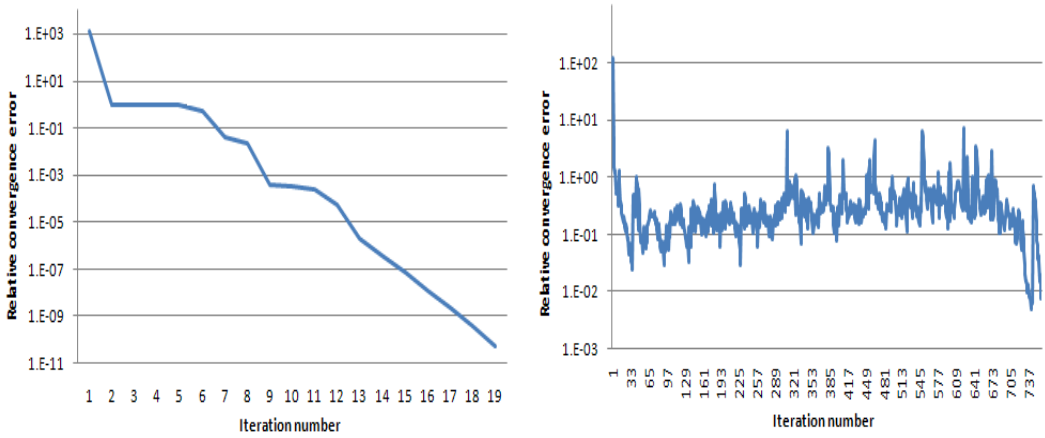


Figure 5: Convergence histories *(left)* FEM with Kirchhoff transformation; *(right)* standard FEM without Kirchhoff transformation.

**Case 1: $C_{\text{in}}$=14 mol/m$^3$, $u_{\text{in}}$=3 m/s, average current density I=1.5Acm$^{-2}$.** Provided that a practical boundary condition $C_{\text{in}}=14mol/m^3, u_{\text{in}}=3m/s$ is reinforced at the inlet of gas channel, and liquid water mass flux condition (2.7) is assigned at membrane/cathode surface with the average cell current density $(I_1+I_2)/2=1.5\text{Acm}^{-2}$, we gain reasonable physical solutions by employing numerical discretization (4.5) and appropriately choos-

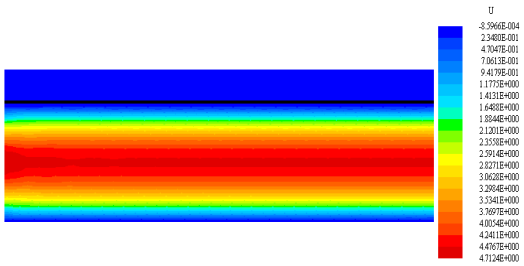

Figure 6: Horizontal two-phase mixture velocity in the case of $C_{\text{in}}=14mol/m^3, u_{\text{in}}=3m/s, I=1.5\text{Acm}^{-2}$.

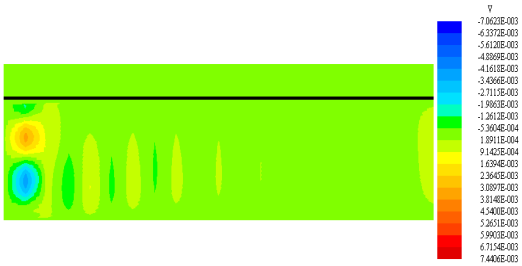

Figure 7: Vertical two-phase mixture velocity in the case of $C_{\text{in}}=14mol/m^3, u_{\text{in}}=3m/s, I=1.5\text{Acm}^{-2}$.

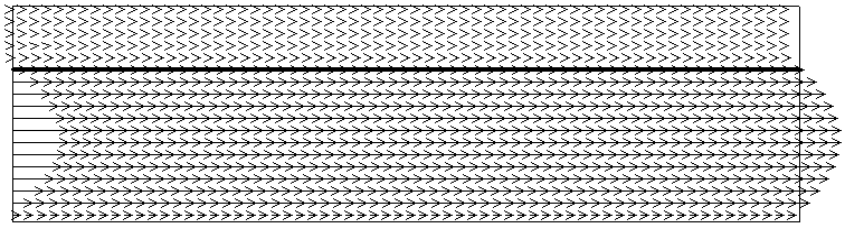

Figure 8: Two-phase mixture velocity field in the case of $C_{\text{in}}=14mol/m^3, u_{\text{in}}=3m/s, I=1.5\text{Acm}^{-2}$.

ing parameters $C_{gls}$ and $C_{sld}$ for nearly optimal control on dominant convectional coefficients. These results are quite similar with [32], see Figs. 6-12 within only 19 nonlinear iteration steps. Fig. 5 displays the fast convergence process with *Kirchhoff* transformation and oscillating iteration without *Kirchhoff* transformation, respectively.

In the following, the focus is placed on elucidating numerical simulation results shown in Figs. 6-12, where the interface of gas channel and GDL is indicated in these figures by a bold line.

Figs. 6-8 shows the velocity field of the two-phase mixture in the GDL and gas channel. As expected, there is a large difference in the velocity scale between the porous GDL and the open channel. The mixture velocity in porous GDL is at least two orders of magnitude smaller than that in the open gas channel, indicating that gas diffusion is the dominant transport mechanism in porous GDL. The flow field in the open channel is fully developed in view of the large aspect ratio of the channel length to width, as can be seen in Fig. 8 where the channel length is, however, not drown to scale for better view.

Fig. 10 displays the water concentration distribution whose value is below $C_{\text{sat}}$, presenting in the phase of water vapor, in the porous cathode and flow channel. As the air flows down the channel, water vapor is continuously added from the cathode, resulting in an increased water vapor concentration along the channel. As a result, liquid water may first appear in the vicinity of the membrane/cathode interface near the channel outlet. A two-phase zone at this location is indeed predicted in the present simulation shown in Fig. 9, where the water concentration is greater than $C_{\text{sat}}$, and water vapor is condensed into liquid water therein.

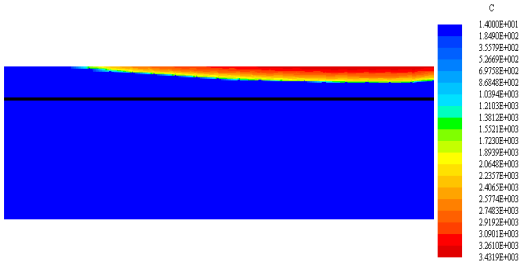

Figure 9: Concentration in the case of $C_{\text{in}} = 14mol/m^3, u_{\text{in}} = 3m/s, I = 1.5\text{Acm}^{-2}$.

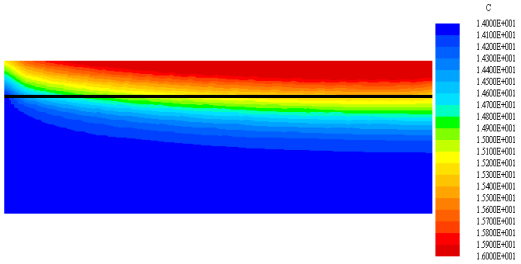

Figure 10: Water vapor concentration in the case of $C_{\text{in}} = 14mol/m^3, u_{\text{in}} = 3m/s, I = 1.5\text{Acm}^{-2}$.

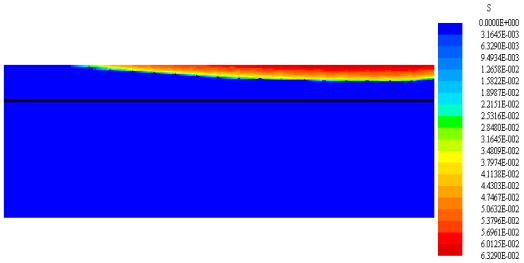

Figure 11: Liquid water saturation in the case of $C_{\text{in}} = 14mol/m^3, u_{\text{in}} = 3m/s, I = 1.5\text{Acm}^{-2}$. The evaporation front separating the two-phase zone from the single-phase region is approximately represented by $s = 0.01$.

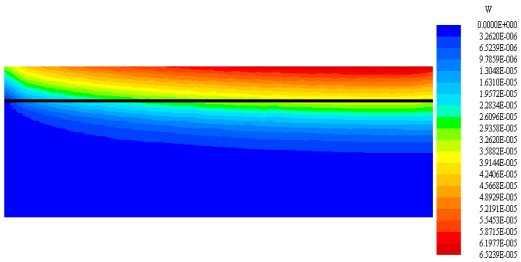

Figure 12: *Kirchhoff*'s variable $W$ in the case of $C_{\text{in}} = 14mol/m^3, u_{\text{in}} = 3m/s, I = 1.5\text{Acm}^{-2}$.

In accordance with Fig. 9, liquid water is seen in the upper-right corner of Fig. 11 to coexist with the saturated water vapor. The largest liquid amount predicted in Fig. 11 is around 6.8% at the average current density of 1.5 A cm$^{-2}$, matching well with 6.3% at the current density of 1.4 A cm$^{-2}$ in [32] where a full PEFC model is considered and the current density $I$ is exactly computed in terms of *Butler-Volmer* equation.

Fig. 12 demonstrates that the *Kirchhoff*'s variable $W$ is a complete smooth function in the porous cathode and flow channel. With the inverse *Kirchhoff* transformation, the postprocessing computation of water concentration $C$ is appropriately achieved in terms of smooth *Kirchhoff*'s variable $W$. Due to the discontinuous and degenerate diffusivity $\Gamma(C)$, the inverse *Kirchhoff* transformation gives birth to water concentration $C$ with sharp interface between single- and two-phase region, suddenly jumping from $C < C_{\text{sat}} = 16$ to the magnitude of $10^3$, as shown in Fig. 9.

**The error of mass balance.** In order to verify the correctness of our numerical solutions, we compute the relative error of mass balance in terms of the numerical fluxes at the inlet and outlet and the source as follows

$$\text{mass balance error} = \frac{\left| \int_{(\partial\Omega)_{\text{outlet}}} C u_1 d\tau - \int_{(\partial\Omega)_{\text{inlet}}} C_{\text{in}} u_1|_{\text{inlet}} d\tau - \frac{I_1+I_2}{4F} l_{\text{PEFC}} \right|}{\int_{(\partial\Omega)_{\text{inlet}}} C_{\text{in}} u_1|_{\text{inlet}} d\tau}. \tag{5.1}$$

By plugging assigned and computed concentration $C$ as well as horizontal velocity $u_1$

Table 2: Convergent mass balance error for the case of $C_{\text{in}}=14mol/m^3, u_{\text{in}}=3m/s, I=1.5Acm^{-2}$.

| Mesh size $h$ | Mass balance error |
|---|---|
| $1.4\times10^{-2}$ | $9.801\times10^{-2}$ |
| $7\times10^{-3}$ | $2.268\times10^{-2}$ |
| $3.5\times10^{-3}$ | $3.088\times10^{-3}$ |

into (5.1), and computing those integrals in terms of one simple numerical quadrature, say, trapezoidal quadrature rule, we attain a convergent mass balance error for our numerical solutions along with the decreasing maximum mesh size $h$, as shown in Table 2. We see that, at current mesh density ($h=3.5\times10^{-3}$), an accurate mass balance error ($<1\%$) is attained for the gained numerical solutions.

**Case 2: $C_{\text{in}}$=14 mol/m$^3$, $u_{\text{in}}$=3 m/s, average current density I=1.05Acm$^{-2}$**. Keep the same entry concentration and velocity with *Case 1* at the inlet, we reduce the average current density to $1.05Acm^{-2}$ by taking $I_1=1.4Acm^{-2}$ and $I_2=0.7Acm^{-2}$ in this case. By our discussion in *Case 1*, this case supposes to lift up the interface between single- and two-phase regions, which means, less liquid water will accumulate near the membrane/cathode surface. By numerically simulating this case within 19 convergent iteration steps, we attain the expected numerical solutions that strongly supports our analysis. In comparison with *Case 1*, there are much smaller amount of liquid water accumulate at the upper right corner of GDL, as displayed in Fig. 13.

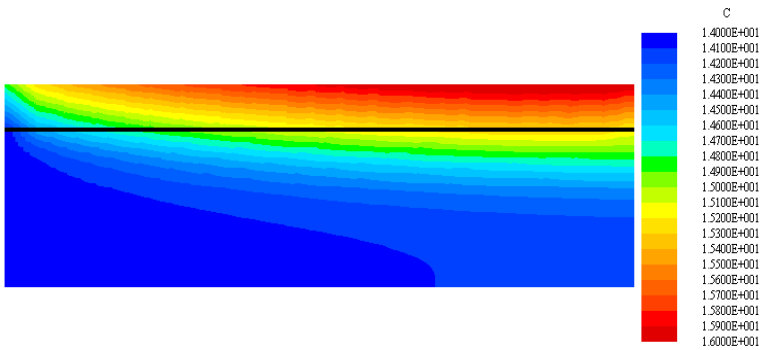


Figure 13: Water vapor concentration in the case of $C_{\text{in}}=14mol/m^3, u_{\text{in}}=3m/s, I=1.05\text{Acm}^{-2}$.

## 6 Conclusions

Many numerical experiments indicate that the main difficulty in the numerical simulation of two-phase transport model in the cathode of polymer electrolyte fuel cell is the oscillating nonlinear iteration. We investigate this problem and found that the discontinuous and degenerate diffusivity in concentration equation and the dominant convection

coefficients in gas channel are two crucial reasons to prevent the entire nonlinear iteration from convergence.

In our numerical efforts on concentration equations (2.4), we present that *Kirchhoff* transformation performs dramatically on solving discontinuous degenerate concentration equation in GDL. In terms of different *Kirchhoff* transformation in GDL and gas channel, we reformulate (2.4) to a convection diffusion equation with simple *Laplacian* term as diffusion and different treatments on convection terms.

To handle dominant convection coefficients in gas channel, we employ *Galerkin*-least-squares method for Navier-Stokes equation and streamline-diffusion scheme for water concentration equation in our finite element approximations. Fast and convergent nonlinear iteration as well as accurate physical solutions are attained, against oscillating iterations with standard finite element and finite volume method and standard linearizations.

Procedures developed in this work are valid only for dry gas channel, where the diffusivity of original water concentration equation (2.4) as well as *Kirchhoff*'s variable $W$ of reformulated water concentration equation (3.5) are mathematically continuous across GDL/gas channel interface.

## Acknowledgments

This work was supported in part by NSF DMS-0609727 and by the Center for Computational Mathematics and Applications of Penn State University. J. Xu was also supported in part by NSFC-10501001 and Alexander H. Humboldt Foundation.

### References

[1] H. W. Alt and S. Luckhaus. Quasilinear elliptic-parabolic differential equations. Math. Z., 183:311–341, 1983.

[2] T. Arbogast, M.F. Wheeler, and N. Zhang. A nonlinear mixed finite element method for a degenerate parabolic equation arising in flow in porous media. SIAM J. Numer. Anal., 33:1669–1687, 1996.

[3] D. N. Arnold. Mixed finite element methods for elliptic problems. Comput. Methods Appl. Mech. Engrg., 82:281–300, 1990.

[4] G. Beavers and D. Joseph. Boundary conditions at a naturally impermeable wall. J. Fluid Mech., 30:197–207, 1967.

[5] J. Crank. Free and Moving Boundary Problems. Clarendon Press, 1984.

[6] R. E. Ewing, O. P. Iliev, and R. D. Lazarov. Numerical simulation of contamination transport due to flow in liquid and porous media. Technical Report 1992-10, Enhanced Oil Recovery Institute, University of Wyoming, 1992.

[7] N. R. Eyres, D.R. Hartree, J. Ingham, R. Jackson, R. J. Sarjant, and S. M. Wagstaff. Phi. Trans. R. Soc, A240:1–57, 1946.

[8] Y. Fan, R. Tanner, and N. Phan-Thien. Galerkin/least-square finite-element methods for steady viscoelastic flows. Journal of Non-Newtonian Fluid Mechanics, 84:233–256, 1999.

[9] L. P. Franca and T. J. R. Hughes. Convergence analyses of galerkin least-square methods for symmetric advective-diffusive forms of the stokes and imcompressible navier-stokes equations. Computer Methods in Applied Mechanics and Engineering, 105:285–298, 1993.
[10] W. Jäger and A. Mikelić. On the interface boundary condition of Beavers, Joseph, and Saffman. SIAM J. Appl. Math., 60:1111–1127, 2000.
[11] C. Johnson, A. H. Schatz, and L. B. Wahlbin. Crosswind smear and pointwise errors in streamline diffusion finite element methods. Math. Comp., 49:25–38, 1987.
[12] T. Kang and D. Yu. Some a posteriori error estimates of the finite-difference streamline-diffusion method for convection-dominated diffusion equations. Advances in Computational Mathematics, 15:193–218, 2001.
[13] N. Kladias and V. Prasad. Experimental verification of darcy-brinkman-forchheimer flow model for natural convection in porous media. J. Thermophys Heat Transfer, 5:560–576, 1991.
[14] K. Niijima. Pointwise error estimates for a streamline diffusion finite element scheme. Numer. Math, 56:707–719, 1990.
[15] U. Pasaogullari and C. Y. Wang. Two-phase modeling and flooding prediction of polymer electrolyte fuel cells. J. Electrochem. Soc, 152:A380–A390, 2005.
[16] A. Quarteroni and A. Valli. Numerical Approximation of Partial Differential Equations, volume 23. Springer Series in Computational Mathematics, 1997.
[17] H. G. Roos and H. Zarin. The streamline-diffusion method for a convection-diffusion problem with a point source. J. Comput. Appl. Math., 150:109–128, 2003.
[18] M. Rose. Numerical methods for flows through porous media. I. Math. Comp., 40:435–467, 1983.
[19] P. Saffman. On the boundary condition at the surface of a porous media. Stud. Appl. Math., 50:292–315, 1971.
[20] M. Stynes and L. Tobiska. The SDFEM for a convection-diffusion problem with a boundary layer: Optimal error analysis and enhancement of accuracy. SIAM J. Numer. Anal., 41:1620–1642, 2003.
[21] P. T. Sun and J. C. Xu. Models research in the cathode of PEFC. Technical Report AM317, Computational and Applied Mathematics, Pennsylvania State University, 2007.
[22] P. T. Sun and J. C. Xu. Numerical simulation on two-phase steady-state transport model in PEFC cathode. Technical Report AM318, Computational and Applied Mathematics, Pennsylvania State University, 2007.
[23] P. T. Sun, G. R. Xue, C. Y. Wang, and J. C. Xu. A combined finite element-upwind finite volume method for three dimensional simulations of liquid feed direct methanol fuel cells. Preprint, 2007.
[24] P. T. Sun, G. R. Xue, C. Y. Wang, and J. C. Xu. A domain decomposition method for two-phase transport model in the cathode of polymer electrolyte fuel cell. J. Comput. Phys. (submitted), 2007.
[25] T. E. Tezduyar. Stabilized finite element formulations for incompressible flow computations. Adv. Appl. Mech., 28:1–44, 1992.
[26] L. Thompson and P. Pinsky. A galerkin least-squares finite element method for the two-dimensional helmholtz equation. Int. J. Numer. Methods Eng., 38:371–397, 1994.
[27] V. R. Voller. Numerical treatment of rapidly changing and discontinuous conductivities. Technical Note, Int. J. Heat and Mass Transfer, 44:4553–4556, 2001.
[28] V. R. Voller and C. R. Swaminathan. Treatment of discontinuous thermal conducitivity in control-volume solutions phase-change problems. Numer. Heat Transfer, 24B:161–180, 1993.

[29] C. Y. Wang. Fundamental models for fuel cell engineering. Chem. Rev., 104:4727–4766, 2004.
[30] C. Y. Wang and P. Cheng. Multiphase flow and heat transfer in porous media. Adv. Heat Transfer, 30:93–196, 1997.
[31] C. Y. Wang, Z. H. Wang, and Y. Pan. Two-phase transport in proton exchange membrane fuel cells. In Proc. of Int. Mech. Engr. Congress & Exhibits, Nashville, TN, 1999.
[32] Z. H. Wang, C. Y. Wang, and K. S. Chen. Two-phase flow and transport in the air cathode of proton exchange membrane fuel cells. J. Power Sources, 94:40–50, 2001.
[33] C. S. Woodward and C. N. Dawson. Analysis of expanded mixed finite element methods for a nonlinear parabolic equation modeling flow into variably saturated porous media. Texas Inst. Comp. Appl. Math. University of Texas at Austin, TIACM Report, 96-51, 1996.
[34] X. Xie, J. Xu, and G. Xue. Uniformly stable finite element methods for Darcy-Stokes-Brinkman models. J. Comput. Math., 26:437–455, 2008.